Thermo-poro-mechanics under adsorption applied to the anomalous thermal pressurization of water in undrained clays

Laurent Brochard, Tulio Honorio

Noname manuscript No.
(will be inserted by the editor)

Thermo-poro-mechanics under adsorption applied to the anomalous thermal pressurization of water in undrained clays

Laurent Brochard · Túlio Honório

Received: date / Accepted: date

Abstract Pore fluid pressurization, one of the main causes of soil instability, is known to be anomalously high for interstitial water in clay submitted to undrained heating. This anomaly is attributed to the confinement of water in nanometric micropores. In this work, we use molecular simulation to investigate how confinement affects the thermo-mechanical properties of water and we use a new poromechanical formulation [5] to relate these confined properties to the macroscopic pressurization of water during undrained heating. This new formulation considers the effects of confinement on the thermo-mechanical moduli of water in micropores, and, in particular, it accounts for the break of extensivity with respect to the volume (Gibbs-Duhem equation not valid). The predictions regarding water thermal pressurization are consistent with the available experimental data when considering a double porosity medium (micro- and macro-pores) with osmotic equilibrium between the porosities. It suggests that the excess fluid pressurization arises from the drainage of water from the micro-porosity to the macro-porosity. The proposed poromechanics offers the first quantitative thermo-hydro-mechanical description of clay based on the physics of adsorption with wide perspectives for applications and transposition to other adsorption-sensitive materials (cement-based materials, wood, bones, microporous carbons etc.).

L. Brochard
Laboratoire Navier (UMR 8205), ENPC, Univ. Gustave Eiffel, CNRS, 6 & 8 avenue Blaise Pascal, 77455 Marne-la-Vallée, France
E-mail: laurent.brochard@enpc.fr

T. Honório
Université Paris-Saclay, ENS Paris-Saclay, CNRS, LMT - Laboratoire de Mécanique et Technologie, 94235, Cachan, France

Keywords clay · water pressurization · drainage · poromechanics · adsorption

1 Introduction

Water, the most common liquid on Earth, is ubiquitous in soils and rocks. Groundwater is a vital resource representing 30 % of all fresh water and it is key for a wide variety of geological processes from faulting and landslide to weathering. In particular, water strongly affects the mechanics of clay-rich soils, notably swelling clay hydration induces large deformations. This phenomenon is the consequence of the strong confinement of water in nanometer-large pores [3]. While the fundamentals behind swelling are reasonably well explained through the concept of disjoining pressure [18, 33, 17], other properties of confined water are still poorly understood. One such property is thermal pressurization. Geomechanical experiments have shown that when saturated clay is submitted to undrained heating, the pressurization of interstitial water exceeds what would be expected from usual poromechanics [26] (see Figure 1). The experiment of thermal pressurization as it is usually performed in geomechanics is a measure of the increase of the interstitial pressure (water pressure) when an undrained sample is heated under constant confining stress. According to usual poromechanics, water pressurization during undrained heating is proportional to the difference between the fluid and solid thermal expansions. A possible interpretation to explain the discrepancy between poromechanics and experiment, is that water adsorption in clay leads to an anomalously high thermal expansion of the fluid [26] (see Figure 1). Interestingly, similar water thermal expansion anomalies have been reported in the literature for other mi-

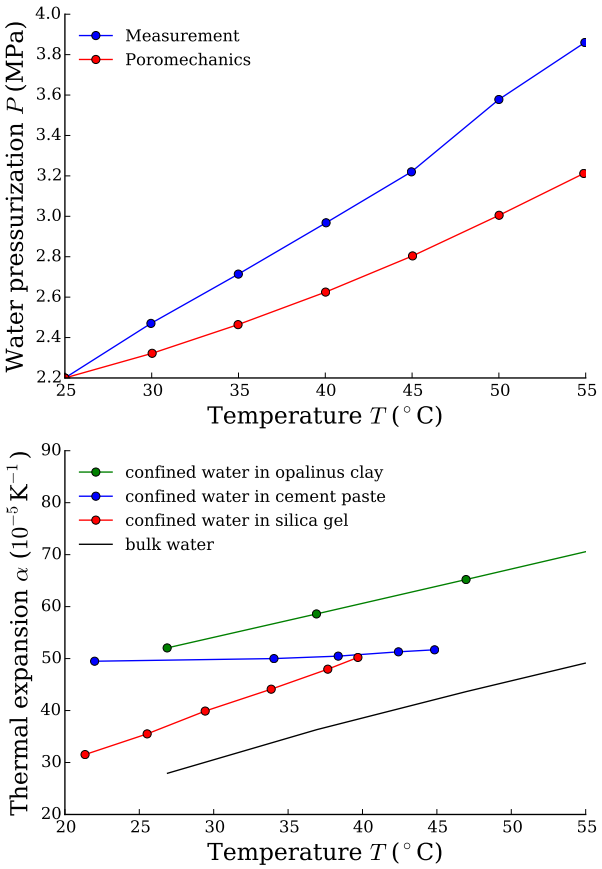

Fig. 1 (top) Interstitial water pressurization in Opalinus Clay during an undrained heating experiments and compared to the prediction with usual poromechanics assuming bulk properties for water (adapted from [26]). (bottom) Experimental results showing the anomalous thermal expansion of confined water (adapted from [26] with data from [40] and [16]).

croporous materials. Early evidence of the anomalous thermal behavior of confined water were obtained in the 1960's for water in silica gels and in titanium oxide powders [12, 13]. More recent investigations have focused on cement paste [36, 16, 15] and porous silica [40, 14, 39] (Figure 1). Understanding water thermal pressurization is key for a variety of applications, since it can trigger instabilities such as shear bands or cracking. For instance, typical values reported in the literature for cement paste are circa 0.5 MPa.K^{-1} [16]; that is, even modest temperature changes can generate megapascals of pressure rapidly exceeding material resistance. This is particularly critical for applications with sudden temperature changes such as geothermal energy, oil well cements [7], or concrete structures under thermal stresses. This is also of critical importance for the understanding of natural instabilities such as earthquakes triggered by clay faults [9].

How confinement impacts the thermo-mechanical properties of a fluid has been investigated by molecular simulation techniques for both idealized systems [29, 28] and realistic ones: porous silica [14, 39] and cement paste [4, 23]. Oleinikova and Brovchenko [28] show that the thermal expansion of hydration water at the surface of model Lennard-Jones solutes is closely anti-correlated with the density. The confined thermal expansion can be several times larger or smaller than the bulk thermal expansion for hydrophobic and hydrophilic surfaces, respectively. More precisely for hydrophilic surfaces (case of interest for clays), the confined thermal expansion is lower than the bulk thermal expansion except at low temperatures (below 350-400K). Thermal expansion is not the only fluid property affected by confinement. Notably, the results of [28] also suggest that confined water is less compressible than bulk water (hydrophilic case), which is of particular interest for thermal pressurization. The interpretation of [26], which attributes the pressurization to water thermal expansion only, disregards other potential effects of confinement such as the change of water compressibility. Regarding more realistic systems, Garofalini et al. [14] investigate the anomalous thermal expansion of water in silica. In this work, anomalous expansion is mostly attributed to the first layer of water at the solid surface, part of which is dissociated, i.e., chemically sorbed. These authors argue that water dissociation is essential to explain the increase in thermal expansion. In the case of Calcium Silicate Hydrates (C-S-H, binding phase of cement-based materials), Bonnaud et al. [4] observe a confined thermal pressurization in mesopores very similar to the bulk thermal pressurization. In the micropores of C-S-H, Krishnan et al. [23] observe that anomalous thermal expansion depends on C-S-H composition and correlates with the level of topological constraint and density of water, whereas water dissociation is not regarded as a primary factor. The results reported for silica and C-S-H are not easily transferable to clays. On one hand, water does not usually dissociate when adsorbed in clay [34, 25]. On the other hand, the concept of topological constraint, relevant for the glassy structure of C-S-H, makes little sense for crystalline clay minerals with layered structure. Clay nano-structure is layered like tobermorite, a crystalline mineral with composition similar to C-S-H (Ca/Si of 1). Following [23], confined water would have a slightly smaller thermal expansion than bulk water, which seems consistent with [28] for hydration water on hydrophilic solid surfaces. Accordingly, the interpretation proposed by Monfared et al. [26] for the undrained heating experiment (anomalously high thermal expansion) is questionable.

In order to understand and predict quantitatively thermal pressurization, one has to know 1- how the thermo-mechanical properties of the confined fluid differ from that of the bulk fluid, and 2- how to upscale those properties from the micropore to the porous medium. In this respect, the framework of poromechanics [10] has been extended to adsorption effect. In the particular case of clay, let us mention the work of Murad and Cushman [27] which proposed a formulation adapted to double porosities (micro- and macro-pores) in non-isothermal conditions, in which the effect of adsorption is accounted for through a contribution of micro-pore size to fluid Helmholtz free energy. Yet, existing formulations rely on Gibbs-Duhem equation (a modified version in the work of [27]), which is not valid for water adsorbed in clays. Gibbs-Duhem equation originates from the extensive behavior of fluids, but the strong confinement of adsorbed water in clay breaks the extensivity. A clear evidence of this observation is the fact that water disjoining pressure isotherm in clay varies with the basal spacing (Fig. 3) [21]; so the pressure of confined water is not only a function of temperature and chemical potential, but also of fluid volume. As we explain in section 2, a major consequence is that 6 moduli are needed in order to fully describe the thermo-mechanical behavior of confined water instead of 3 for usual bulk water (compressibility, thermal expansion, and heat capacity). This fundamental change leads for instance to distinguish the compressibility with respect to the volume and that with respect to the number of molecule. Thus, in isothermal conditions, pressure of confined water has unrelated dependencies in volume and number of molecules, so that it is no more a function of density only like bulk water (Fig. 3). The formulation of poromechanics proposed by Murad and Cushman [27] does recognize an effect of pore size on pressure, but still considers density as a state parameter to describe the confined fluid (Murad and Cushman [27] restrict themselves to large micropores, ~ 10 water layers, for which they reasonably assume the same density for the bulk and adsorbed water). This leads to a modified Gibbs-Duhem equation that imposes constraints on the thermo-mechanical description of the fluid. We proposed recently a new formulation of poromechanics extended to adsorption that does not assume Gibbs-Duhem equation for the confined fluid [5]. In particular, we showed that assuming Gibbs-Duhem or not is critical for the phenomenon of fluid thermal pressurization in undrained conditions: assuming Gibbs-Duhem equation leads to an expression very close to usual poromechanics (which is known to significantly underestimate the experiments of Monfared et al. [26]), whereas not assuming Gibbs-Duhem equation significantly changes the expression of pressurization which may provide an explanation for the case of water in clays. Yet, any quantitative application of this new theory requires to first provide estimates of all 6 thermo-mechanical moduli except heat capacity, at a scale hardly accessible to experiments. In this paper, we use molecular simulation techniques to do so and we apply quantitatively the new poromechanics to the undrained heating test.

In section 2, we recall the new undrained thermo-poro-mechanics [5] and we derive from it the expression of thermal pressurization during undrained heating. Section 3 is dedicated to the molecular simulations and estimates of confined water properties. We highlight the peculiarity of water by comparing with a model Lennard-Jones fluid confined in a slit pore. Finally, in section 4, we apply the new thermo-poromechanics and confront the results to the experimental thermal pressurization of Monfared et al. [26].

2 Poromechanical derivation of water thermal pressurization

Let us consider a porous medium submitted to the undrained heating experiment of Monfared et al. [26]. This experiment consists in measuring the increase of fluid pressure when the porous medium is subjected to an increase of temperature T while the amount of fluid $\phi\rho$ in the medium (ϕ is the porosity, ρ is the fluid density in the pores) and confining stress σ are held constant. Practical measurement of fluid pressure always refers to the bulk fluid pressure P_b in osmotic equilibrium with all the fluid in the pores: pressure is not measured within a micropore, but the fluid confined in micropores and the bulk fluid in larger pores share the same chemical potential μ and temperature T. Accordingly, the quantity which is measured is $\frac{\partial P_b}{\partial T}\big|_{\sigma,\phi\rho}$. The appropriate thermodynamic quantity characterizing the fluid in the pore is not the pressure since micropore pressure and bulk pressure can differ due to fluid confinement in micropores. Chemical potential is the appropriate quantity since osmotic equilibrium ensures equality of the chemical potential throughout the porosity. The derivative of bulk fluid pressure with respect to temperature can be related to a derivative of chemical potential μ thanks to Gibbs-Duhem equation:

$$\left.\frac{\partial P_b}{\partial T}\right|_{\sigma,\phi\rho} = \rho_b \left.\frac{\partial \mu}{\partial T}\right|_{\sigma,\phi\rho} + s_b \tag{1}$$

where ρ_b and s_b are the bulk fluid density and entropy per unit volume. In order to relate this derivative to the fluid and solid properties, one needs a constitutive description of the porous medium relating fluid

chemical potential to temperature, confining stress and amount of fluid. Poromechanics [10], which is commonly used in soil and rock mechanics, is well adapted. Hereafter, we derive the thermal pressurization following usual poromechanics [10], and then following the new poromechanics we developed to account for the effect of confinement [5].

In usual poromechanics, the fluid filling the porosity ϕ of a porous medium is supposed to have usual 'bulk' properties: bulk modulus K_b, thermal expansion α_b, and volumetric heat capacity c_b^v. The undrained behavior of a porous medium is given by the following set of constitutive equations relating the changes of spherical stress σ, fluid chemical potential μ, and entropy per unit volume s to the changes of volumetric strain ϵ, amount of fluid $\phi\rho_b$, and temperature T:

$$\begin{cases} d\sigma = K_u d\epsilon - \frac{Mb}{\rho_b} d\left(\phi\rho_b\right) - K_u\alpha_u dT \\ d\mu = -\frac{Mb}{\rho_b} d\epsilon + \frac{M}{\rho_b^2} d\left(\phi\rho_b\right) + \frac{M\alpha_\mu}{\rho_b} dT \\ ds = ds_s + d\left(\phi s_b\right) = K_u\alpha_u d\epsilon - \frac{M\alpha_\mu}{\rho_b} d\left(\phi\rho_b\right) + \frac{c_u}{T} dT \end{cases} \tag{2}$$

where:

- $\frac{1}{M} = \frac{1}{N} + \frac{\phi}{K_b}$ is the undrained Biot modulus (N is the drained Biot modulus),
- b is the Biot coefficient,
- $K_u = K + Mb^2$ is the undrained bulk modulus (with K the drained bulk modulus),
- $K_u\alpha_u = K\alpha_s + Mb\alpha_{\rho\phi}$ is the undrained thermal rigidity (with α_s the thermal expansion of the solid skeleton, $\alpha_{\rho\phi} = \alpha_\phi + \phi\alpha_b$ the thermal expansion of the fluid-solid mixture, and $\alpha_\phi = \alpha_s\left(b-\phi\right)$),
- $M\alpha_\mu = M\alpha_{\rho\phi} - s_b$ is the undrained thermo-chemical coupling coefficient (with s_b the fluid entropy per unit volume),
- $\frac{c_u}{T} = \frac{c+\phi c_b^v}{T} + \frac{K_b}{\phi}\left(\phi\alpha_b\right)^2 - M\alpha_{\rho\phi}^2$ is the undrained heat capacity (with c the drained heat capacity).

Combining the constitutive equations (2) of usual poromechanics with the expression of thermal pressurization (Eq. 1), one obtains the following expression of fluid thermal pressurization:

$$\left.\frac{\partial P_b}{\partial T}\right|_{\sigma,\phi\rho_b} = \frac{KM\phi}{K_u}\left(\alpha_b - \alpha_s\right) = \frac{\phi\left(\alpha_b - \alpha_s\right)}{1/M + b^2/K} \tag{3}$$

Applying this relation, Monfared et al. [26] predict a thermal pressurization much smaller than that measured (see Figure 1 top). Conversely, one can invert equation (3) to estimate what should be the value of the fluid thermal expansion (α_b) that can lead to the measured thermal pressurization. Doing so leads to the anomalously high thermal expansion of water reported in Figure 1 (bottom). As discussed in the introduction, this back analysis is somewhat questionable since it assumes that the fluid thermal expansion is the only parameter which is impacted by confinement. The expression (3) of thermal pressurization involves another fluid property (K_b) which can also be affected by confinement. The consequences of confinement are even more complex since the non-validity of Gibbs-Duhem equation in micro-pores requires introducing additional fluid properties. We addressed this issue by proposing a new formulation of poromechanics adapted to confined fluids without assuming Gibbs-Duhem equation [5]. In this new formulation, the thermo-mechanical description of the fluid confined in micropores requires to introduce a total of 6 thermo-mechanical moduli:

1. the drained bulk modulus $K^d = -V\left.\frac{\partial P}{\partial V}\right|_{\mu,T}$
2. the undrained bulk modulus $K^V = -V\left.\frac{\partial P}{\partial V}\right|_{N,T}$
3. the rigidity with respect to the number of particles at constant volume and temperature $K^N = -N\left.\frac{\partial P}{\partial N}\right|_{V,T}$
4. the drained thermal expansion $\alpha^d = \frac{1}{V}\left.\frac{\partial V}{\partial T}\right|_{P,P_b}$
5. the undrained thermal expansion $\alpha^u = \frac{1}{V}\left.\frac{\partial V}{\partial T}\right|_{N,P}$
6. the volumetric heat capacity c^v.

The special case of a fluid following Gibbs-Duhem equation corresponds to $K^d = 0$, $K^V = K^N$, and $K^d\alpha^d = 0$; so that one is left with a usual fluid description involving only 3 independent moduli. For the sake of reability, in what follows, we use the following notations : $K_c = K^N$ (subscript $_c$ for 'confined'), $\gamma = \frac{K^V - K^d}{K^N}$, and $\delta = \frac{K^V}{K^N}$. Therefore, assuming Gibbs-Duhem equation is equivalent to considering $\gamma = 1$, $\delta = 1$, and $\left(\delta-\gamma\right)\alpha^d = 0$. Let us now consider a micro-porous medium in which the fluid in the pores is described by this new set of properties. Adapting the derivation of poromechanics to this new paradigm, the set of constitutive equations (2) becomes [5]:

$$\begin{cases} d\sigma = K_u^{eff} d\epsilon - \frac{M^{eff} b^{eff}}{\rho_b} d\left(\phi\rho_c\right) - K_u^{eff}\alpha_u^{eff} dT \\ d\mu = -\frac{M^{eff} b^{eff}}{\rho_b} d\epsilon + \frac{M^{eff}}{\rho_b^2} d\left(\phi\rho_c\right) + \frac{M^{eff}\alpha_\mu^{eff}}{\rho_b} dT \\ ds = K_u^{eff}\alpha_u^{eff} d\epsilon - \frac{M^{eff}\alpha_\mu^{eff}}{\rho_b} d\left(\phi\rho_c\right) + \frac{c_u^{eff}}{T} dT \end{cases} \tag{4}$$

where:

- $M^{eff} = \frac{\mathcal{M}^{eff}}{\beta}\left(\frac{\rho_b}{\delta\rho_c}\right)^2$ is the effective undrained Biot modulus (with $\frac{1}{\mathcal{M}^{eff}} = \frac{1}{N} + \frac{\phi}{\delta K_c}$),
- $b^{eff} = \frac{\beta b\delta\rho_c}{\rho_b}$ is the effective drained Biot coefficient (with $\beta = \frac{\gamma}{\delta-\gamma}\frac{\phi M^d}{\delta K_c}$ and $\frac{1}{M^d} = \frac{1}{N} + \frac{1}{\delta-\gamma}\frac{\phi}{K_c}$),

- $K_u^{eff} = K^{eff} + M^{eff}\left(b^{eff}\right)^2$ is the effective undrained bulk modulus (with $K^{eff} = K + M^d b^2$ the effective drained bulk modulus),
- $K_u^{eff}\alpha_u^{eff} = K\alpha_s + \frac{M^{eff}b^{eff}}{\beta}\alpha_{\rho\phi}^{eff}$ is the effective undrained thermal rigidity (with $\alpha_{\rho\phi}^{eff} = \beta\frac{\delta\rho_c}{\rho_b}\left(\alpha_\phi + \phi\alpha_c^u\right)$ the effective thermal expansion of the fluid-solid mixture),
- $\alpha_\mu^{eff} = \alpha_{\rho\phi}^{eff} + \delta\left(1-\beta\right)\phi^{eff}\left(\alpha_c^u - \alpha_c^d\right) - \frac{s_b}{M^{eff}}$ is the effective undrained thermo-chemical coupling coefficient (with $\phi^{eff} = \frac{\phi\rho_c}{\rho_b}$ an effective (apparent) porosity),
- and $\frac{c_u^{eff}}{T} = \frac{c+\phi c_c^v}{T} + \frac{\delta K_c}{\phi}\left(\phi\alpha_c^u\right)^2 - \frac{M^{eff}}{\beta}\left(\alpha_{\rho\phi}^{eff}\right)^2$ is the effective undrained heat capacity.

Based on this new formulation of poromechanics, one obtains the following expression of the thermal pressurization (Eq. 1):

$$\left.\frac{\partial P_b}{\partial T}\right|_{\sigma,\phi\rho_c} = \overbrace{\frac{\rho_b}{\delta\rho_c}}^{\left.\frac{\partial P_b}{\partial P_c}\right|_{T,\phi\rho_c}} \overbrace{\frac{K\mathcal{M}^{eff}}{K_u^{eff}}\phi\left(\alpha_c^u - \alpha\right)}^{\left.\frac{\partial P_c}{\partial T}\right|_{\sigma,\phi\rho_c}} + \underbrace{\frac{\rho_b}{\rho_c}\frac{\delta-\gamma}{\gamma}K_c\left(\alpha_c^u - \alpha_c^d\right)}_{\left.\frac{\partial P_b}{\partial T}\right|_{P_c,\phi\rho_c}} \quad (5)$$

Comparing this expression of thermal pressurization to the usual one (Eq. 3), it appears that the effect of confinement is much more complex than just the change of thermal expansion ($\alpha_b \rightarrow \alpha_c^u$). One can interpret the different contributions as a combination of partial derivatives. The first term combines the increase of bulk pressure due to the increase of confined pressure with the increase of confined pressure due to undrained heating. This term is analogous to the usual expression (Eq 3), but involves the effective properties of the porous medium and a multiplicative factor corresponding to the relative increase between bulk and confined pressures at constant temperature. The second term on the right hand side is much less intuitive, primarily because it does not depend on the porous solid moduli or even on the porosity. Carefully analyzing the confined fluid behavior, one can interpret this term as the increase of bulk pressure with temperature at constant confined pressure and amount of fluid. This phenomenon arises from a mismatch between the thermal expansion at constant bulk pressure and at constant confined pressure : $\frac{\delta-\gamma}{\gamma}\left(\alpha_c^u - \alpha_c^d\right) = \frac{1}{V_c}\left.\frac{\partial V_c}{\partial T}\right|_{P_b,\phi\rho_c} - \frac{1}{V_c}\left.\frac{\partial V_c}{\partial T}\right|_{P_c,\phi\rho_c}$. This contribution to thermal pressurization is intrinsic to the confined fluid and holds irrespective of the poromechanical properties of the solid or of the porosity.

How confinement impacts thermal pressurization is therefore quite complex. A high confined density with respect to the bulk tends to reduce the thermal pressurization. The effect of the other unusual factors (γ, δ, α_c^u and α_c^d) is hard to anticipate unless typical values are considered. Since $\gamma < \delta$ and we typically expect $\alpha_c^u > \alpha_c^d > 0$ for clays, one can expect a positive contribution of the second term of Equation (5), i.e., an increase of the thermal pressurization. The magnitude of the second contribution scales with the confined modulus K_c, i.e., it is of similar magnitude as the first contribution. Therefore, the effect of confinement can be major. Further analysis requires a quantitative application with realistic values of the various parameters, which is the focus of section 4.

It is interesting to investigate the special case where Gibbs-Duhem equation would apply to the confined fluid ($\gamma = 1$, $\delta = 1$, and $(\delta - \gamma)\,\alpha^d = 0$). In that case, the expression of thermal pressurization is dramatically simplified and one gets an expression very close to that of usual poromechanics:

$$\left.\frac{\partial P_b}{\partial T}\right|_{\sigma,\phi\rho} = \frac{\rho_b}{\rho_c}\frac{KM\phi}{K_u}\left(\alpha_c^u - \alpha_s\right) \quad (6)$$

The expression is identical to that of usual poromechanics (Eq. 3) with a prefactor involving the ratio between bulk and confined densities. As mentioned in the introduction, existing literature on properties of adsorbed water in hydrophilic solids suggests that, in the range of temperature of interest, thermal expansion α_c^u and density ρ_c are only little affected by confinement whereas compressibility $1/K_c$ is significantly reduced. Accordingly, following equation (6), the main impact of confinement would be an increase of the undrained bluk modulus K_u, that is a decrease of thermal pressurization, which would be inconsistent with experimental measurements. Therefore, considering Gibbs-Duhem equation valid or not seems of critical importance to explain the undrained heating experiment.

The poromechanical formulation (4) considers that all the fluid in the pores is confined. But many microporous materials, including clay, also contain macropores in which the fluid is bulk. Confined and bulk fluids are in osmotic equilibrium and the fluid transfers between the two porosities may be important in the undrained heating experiment. To address this question, we adapted the poromechanical formulation to double porosity media. The constitutive equations of a double porosity medium (micro- and macro-porosites) in undrained conditions are:

$$\begin{cases} d\sigma = \tilde{K'}_u^{eff} d\epsilon - \frac{\tilde{M}^{eff}\tilde{b}^{eff}}{\rho_b} d\left(\phi\rho\right)_{tot} - \tilde{K'}_u^{eff}\tilde{\alpha'}_u^{eff} dT \\ d\mu = -\frac{\tilde{M}^{eff}\tilde{b}^{eff}}{\rho_b} d\epsilon + \frac{\tilde{M}^{eff}}{\rho_b^2} d\left(\phi\rho\right)_{tot} + \frac{\tilde{M}^{eff}\tilde{\alpha'}_\mu^{eff}}{\rho_b} dT \\ ds = \tilde{K'}_u^{eff}\tilde{\alpha'}_u^{eff} d\epsilon - \frac{\tilde{M}^{eff}\tilde{\alpha'}_\mu^{eff}}{\rho_b} d\left(\phi\rho\right)_{tot} + \frac{\tilde{c'}_u^{eff}}{T} dT \end{cases} \tag{7}$$

where

- $\tilde{b}^{eff} = b_b + \tilde{\beta}\frac{\delta\rho_c}{\rho_b} b_c$ is the effective Biot coefficient (with $\tilde{\beta} = \tilde{M}^d\left(\frac{\gamma}{\delta-\gamma}\frac{\phi_c}{\delta K_c} - \frac{\rho_b}{\delta\rho_c}\frac{1}{N_{bc}}\right)$ and $\frac{1}{\tilde{M}^d} = \frac{1}{N_{cc}} + \frac{1}{\delta-\gamma}\frac{\phi_c}{K_c}$),
- $\frac{1}{\tilde{M}^{eff}} = \frac{1}{\tilde{N}^{eff}} + \frac{\tilde{\phi}^{eff}}{K_b}$ is the effective undrained Biot modulus (with $\frac{1}{\tilde{N}^{eff}} = \frac{1}{N_{bb}} - \frac{1}{\tilde{M}^d}\left(\frac{\tilde{\beta}\delta\rho_c}{\rho_b}\right)^2 + \phi_c^{eff}\left(\frac{\delta\gamma}{\delta-\gamma}\frac{\rho_c}{\rho_b}\frac{1}{K_c} - \frac{1}{K_b}\right)$ the effective Biot modulus, $\tilde{\phi}_{eff} = \phi_b + \phi_c\frac{\rho_c}{\rho_b}$ an effective porosity, $\phi_c^{eff} = \phi_c\frac{\rho_c}{\rho_b}$),
- $\tilde{K'}_u^{eff} = \tilde{K}^{eff} + \tilde{M}^{eff}\left(\tilde{b}^{eff}\right)^2$ is the effective undrained bulk modulus (with $\tilde{K}^{eff} = K + \tilde{M}^d b_c^2$ the effective drained bulk modulus),
- $\tilde{K'}_u^{eff}\tilde{\alpha'}_u^{eff} = \tilde{K}^{eff}\tilde{\alpha}^{eff} + \tilde{M}^{eff}\tilde{b}^{eff}\left(\tilde{\alpha}_{\rho\phi}^{eff} + \delta\left(1-\tilde{\beta}\right)\phi_c^{eff}\left(\alpha_c^u - \alpha_c^d\right)\right)$ is the effective undrained thermal rigidity (with $\tilde{K}^{eff}\tilde{\alpha}^{eff} = \tilde{K}^{eff}\alpha_s + \tilde{M}^d b_c\phi_c\left(\alpha_c^d - \alpha\right)$ the effective drained thermal rigidity),
- $\tilde{\alpha'}_\mu^{eff} = \tilde{\alpha}_{\rho\phi}^{eff} + \delta\left(1-\tilde{\beta}\right)\phi_c^{eff}\left(\alpha_c^u - \alpha_c^d\right) - \frac{s_b}{\tilde{M}^{eff}}$ is the effective undrained thermo-chemical coupling coefficient (with $\tilde{\alpha}_{\rho\phi}^{eff} = (\alpha_{\phi_b} + \phi_b\alpha_b) + \tilde{\beta}\frac{\delta\rho_c}{\rho_b}\left(\alpha_{\phi_c} + \phi_c\alpha_c^u\right)$ the effective thermal expansion of the fluid-solid mixture),
- $\frac{\tilde{c'}_u^{eff}}{T}$ is the effective undrained heat capacity (see expression in [5]);

The double porosity poromechanics involves properties of the porous solid specific to each porosity: ϕ_b, ϕ_c, b_b, N_{bb}, α_{ϕ_b}, b_c, N_{cc}, and α_{ϕ_c} are the porosities, Biot coefficients and moduli, and thermal expansions of the macro- and micro-pores, respectively; and N_{bc} is the Biot modulus characterizing the mechanical coupling between the two porosities. Combining the double porosity poromechanics with the expression of the fluid pressurization during undrained heating (1), we obtain:

$$\left.\frac{\partial P_b}{\partial T}\right|_{\sigma,(\phi\rho)_{tot}} = \frac{\tilde{K}^{eff}\tilde{M}^{eff}}{\tilde{K'}_u^{eff}}\left(\phi_b\left(\alpha_b - \alpha\right) + \left(\tilde{\beta}\frac{\delta\rho_c}{\rho_b} - \frac{\tilde{b}^{eff}\tilde{M}^d}{\tilde{K}^{eff}}b_c\right)\phi_c\left(\alpha_c^u - \alpha\right) + \left(\left(1-\tilde{\beta}\right)\frac{\delta\rho_c}{\rho_b} + \frac{\tilde{b}^{eff}\tilde{M}^d}{\tilde{K}^{eff}}b_c\right)\phi_c\left(\alpha_c^u - \alpha_c^d\right)\right) \tag{8}$$

This expression of the thermal pressurization share similarities with the case of the single porosity medium (Eq. 5): there are two contributions for the mismatch of thermal expansion between the fluid and the solid (one per porosity) and a contribution due to the intrinsic pressurization of the confined fluid. However, the different terms are now modulated by complex correction factors that capture the fluid transfers between the porosities, the effect of which is hard to anticipate.

3 Estimation of confined water properties by molecular simulations

The application of the extended poromechanics faces a difficulty. While conventional macroscopic experiments can assess the effective properties (bulk modulus, Biot coefficient and modulus, thermal expansions and heat capacity) and usual state equations provide the bulk fluid properties, estimating the properties of the confined fluid is very challenging. Existing experimental techniques in the literature that claim measurements of confined properties, generally measure an effective property and resort to an inverse analysis based on poromechanics or equivalent theories (see for instance [31, 15, 32, 38]). True measurement at the scale of the confined fluid require experiments with nanometric accuracy such as the surface force apparatus [22], or atomic force microscopy [30]. As an alternative, in this work, we use molecular simulation techniques to estimate the confined properties from the fundamental interactions between atoms and molecules. Recent advances in molecular simulation techniques and models offer realistic descriptions of the nanometric scale even for complex materials such as clays; which conveniently supplement experiments at this scale. All thermo-mechanical properties (K_c^d, K_c^V, K_c^N, α_c^d, α_c^u, and c_c^v) are second order derivatives of appropriate thermodynamic potentials and can be computed either by fluctuation formula or by finite differences. For instance, the thermal expansion can be obtained via the cross-correlation of volume (V) and enthalpy (H) in the isobaric-isothermal ensemble [1] : $\alpha = \langle \Delta V \Delta H \rangle_{NPT} / kT^2 V$, where $\Delta X = X - \langle X \rangle$. And, it can also be estimated by finite differences between two simulations at different temperatures but same pressure : $\alpha = \left(\partial \langle V \rangle / \partial T|_{N,P}\right) / \langle V \rangle$. In this work, we use finite differences, which proves computationally more efficient (fluctuation formula were used for cross-checking only).

To study the confined properties of water in clays, we consider a realistic molecular simulation of Na-montmorillonite (Figure 2). In this simulation, water SPC/E

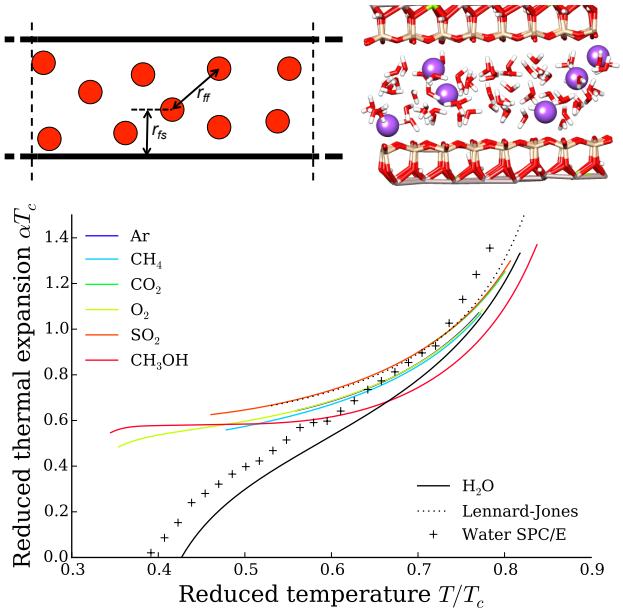

Fig. 2 (top) Representations of the LJ fluid and water confined in a slit pore and in Na-Montmorillonite, respectively. (bottom) Thermal expansion isobars of various liquids as function of temperature at 20% of the critical pressure. A common scale is adopted by reducing thermal expansion and temperature axis with respect to the critical temperature of each liquid. We also include the cases of the water SPC/E model and of the LJ fluid (the accurate EOS of [35] is used for the LJ fluid). Data for the various liquids are from NIST (https://webbook.nist.gov/).

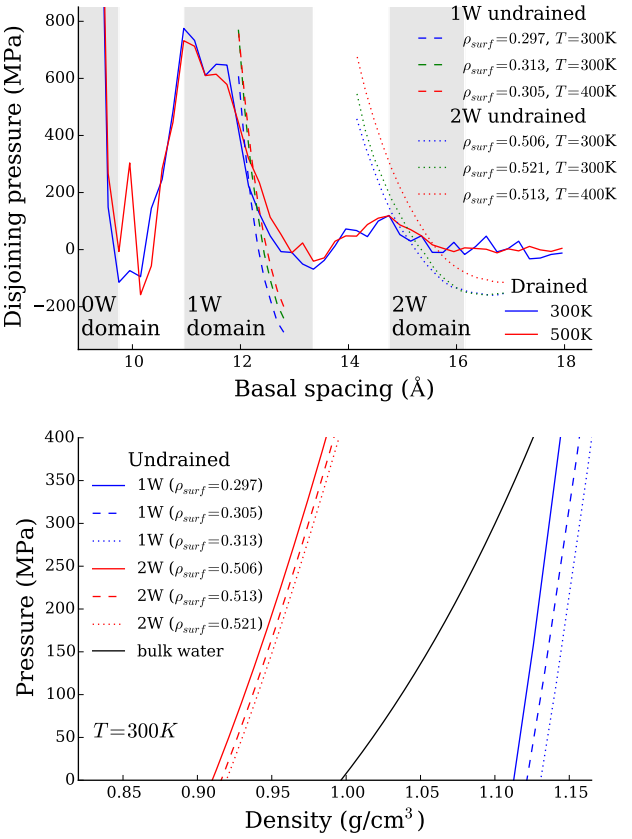

Fig. 3 Illustration of the drained and undrained behaviors of the clay layer. (top) Disjoining pressure as function of the basal spacing. The shaded domains correspond to the stable basal spacings (decreasing branches of the disjoining pressure isotherm), referred to as xW with x the number of water layers in the micropore. The number of water molecules used for the undrained simulations are chosen to be representative of the 1W and 2W states. The dashed and dotted curves show the effect of temperature and number of molecules (undrained case) on the mechanics. (bottom) Undrained pressure-density curves for the 1W and 2W states of water at different amount of surface density ρ_{surf} (amount of water per unit area, in unit of mg/m^2). Because of adsorption, pressure is no more a function of density only, as in the case for bulk water. All molecular simulations were performed following the method described in [21].

[2] and sodium ions are confined between mineral layers of montmorillonite. The ClayFF potential [11] is used to model the interactions with the solid layer. The structural formula is $Na_6[Si_{62}Al_2][Mg_4Al_{28}]O_{160}(OH)_{32}.nH_2O$ (see [8] for the details about the atomic structure employed here). The total charge density of the layers is -0.124 C.m^2. Grand Canonical Monte Carlo and molecular dynamics simulations are performed to obtain the drained and undrained behavior, respectively (see [21] and [20] for details about the simulations). Figure 3 illustrates typical results for both drained and undrained behaviors at different temperatures and number of water molecules (undrained case only).

It is important to note that bulk water has a very unusual behavior regarding thermo-mechanical couplings, and one has to make sure that this unusual behavior is well captured by the molecular model of water we use. Water density is maximum at 4°C, so its thermal expansion is negative below this temperature. Above 4°C, water thermal expansion is positive but significantly smaller than that commonly observed for other liquids. Figure 2 (bottom) compares the thermal expansion of various liquids (non-polar, quadru-polar, di-polar) to that of water as a function of temperature. A common scale is obtained by considering the values of thermal expansion and temperature reduced with respect to the critical temperature of each liquid. Each curve is an isobar at a pressure corresponding to 20% of the critical pressure. Interestingly, all liquids except water follow a single master curve. Water deviates from this master curve and exhibits anomalous thermal expansion at temperatures below $0.6T_c \sim 100$°C. The anomalous behavior of water at low temperatures has long been known and is attributed to the structuring nature of the hydrogen bond network [19, 24]. We display in Figure 2 (bottom) the case of the SPC/E model of water,

which follows well the thermal expansion of real water and deviates from the other liquids at low temperatures. SPC/E is not perfect since it over-estimates a little the thermal expansion of real water, but this is accurate enough to clearly discriminate between the case of conventional liquids and that of water.

For the sake of comparison, we also study the thermo-mechanical properties of a 2D Lennard-Jones (LJ) fluid in a slit pore (Figure 2). A 12-6 LJ fluid ($U_{ff} = 4\varepsilon \left((\sigma/r_{ff})^{12} - (\sigma/r_{ff})^{6} \right)$) is confined in a slit pore made of two straight walls interacting with the fluid through a 9-3 Lennard-Jones potential ($U_{fs} = \varepsilon \left(\frac{2}{15} (\sigma/r_{fs})^{9} - (\sigma/r_{fs})^{3} \right)$). The LJ liquid is an interesting benchmark since its thermo-mechanical behavior is quite representative of that of most liquids (Figure 2). Therefore, confronting LJ and SPC/E should allow us to know whether the anomalous thermal pressurization of interstitial water in clay is a phenomenon common to other confined fluid or specific to water.

In the confined volume of a planar nanometric pore, the fluid density is not uniform, instead one observes a layered structure. Disjoining pressure isotherms obtained in the Grand Canonical ensemble exhibit oscillations (Fig. 3), which means that some basal spacings are mechanically unstable (increasing branches of the isotherms), while others are stable (decreasing branches). One refers to the stable branches as to 'xW' where x is the number of fluid layers, i.e., 0W when there is no fluid, 1W when there is one layer etc.. The realistic model of Na-montmorillonite exhibits 2 water layers [21], whereas the idealized model of the 2D LJ fluid exhibits 5 fluid layers or more [6]. Undrained properties (K_c^V, K_c^N, and α_c^u) are computed at controlled number of fluid molecules, but one must select appropriate numbers of fluid molecules corresponding to stable basal spacings. Since the behavior of a confined fluid may well depend on the number of fluid layers, we considered 1W and 2W for the realistic Na-montmorillonite and 1W, 3W and 5W for the idealistic LJ model. Thus, the results reported in this paper for the confined fluid refer to these 'xW' states.

Another issue is to decide the thickness of the micropore. In the molecular simulation, we impose the basal spacing of the system, which includes the thickness of both the micropore and the solid layer. The solid atoms are considered rigid and one only simulates the interstitial fluid molecules. Therefore, choosing the micropore volume is equivalent to setting the thickness of the solid. Our choice in this paper is to set the thickness of the solid as the value of the basal spacing in the dry state (0W) for which the disjoining pressure at 300K is 0, that is 9.66Å (and 1.4σ for the LJ fluid in a slit pore). This is a rather 'mechanical' definition. Many alternatives definitions are possible, for instance the basal spacing at which water molecules start adsorbing in the micropore ($\sim$ 9.8 Å), or the distance between the centers of the outer-most atoms of the solid plus their respective Lennard-Jones radius (9.58 Å). Anyway, all these choices differ by ± 0.2 Å. To show the impact of this choice on our results, we provide error bars in the thermal pressurization curves of section 4 that corresponds to a ± 0.2 Å uncertainty in the thickness of the solid. Note that the choice of volume of the confined fluid has an impact on the computation of the pressure since it is involved in the virial formula [1], but the product of the pressure by the volume is unambiguous. One can take advantage of this observation to convert the results of one choice of micropore volume V_c to another one V_c'. In the limit of $P_c \ll K_c$, we have : $K_c' = \frac{V_c}{V_c'} K_c$, $\gamma' = \frac{V_c'}{V_c}\gamma$, $\delta' = \frac{V_c'}{V_c}\delta$, $\alpha_c'^u = \frac{V_c}{V_c'}\alpha_c^u$, $\alpha_c'^d = \frac{V_c}{V_c'}\alpha_c^d$, $c_c'^v = \frac{V_c}{V_c'} c_c^v$, and $\rho_c' = \frac{V_c}{V_c'}\rho_c$, where the $'$ refers to the properties corresponding to the choice V_c'. Therefore, it is quite easy to convert the results from one choice of micropore size to another one. For the sake of clarity, we prefer displaying results in term of basal spacing (Figs. 3 and 7), which is the only unambiguous size, but confined properties displayed in Figures 4 and 6 do assume a solid thickness of 9.66Å.

The confined water properties estimated by molecular simulations are provided in Figures 4, 6 and 7. In Figure 4, we report the results of undrained thermal expansion (α_c^u) and undrained thermal rigidity ($\kappa_c = K_c^V \alpha_c^u$). In Figure 6, we report the results of undrained rigidities with respect to volume (K_c^V) and number of molecules (K_c^N). And in Figure 7, we report the drained properties (density, disjoining pressure) from which one can estimate the drained bulk modulus (K_c^d) and drained thermal expansion (α_c^d). We do not report any results of heat capacity since it is not involved in the expression of fluid pressurization during undrained heating (Eq. 8). Based on these results, we can derive the confined water properties listed in Table 1.

Let us analyze first thermal expansion and rigidity (Fig. 4). We display the properties as function of temperature (T) at various confined pressures (P_c). The temperatures and pressures considered correspond to the domain of liquid water (temperatures from 273.14K to 647.3K, and pressures up to a few times the critical pressure $P_{cr} = 22.6$ MPa). We also display the bulk water properties as a reference (for the same temperatures and pressures). For the sake of comparison, we provide in Figure 5 the thermal expansion and rigidities of the LJ fluid confined in a slit pore. Again, the temperatures and pressures considered for the LJ fluid correspond to

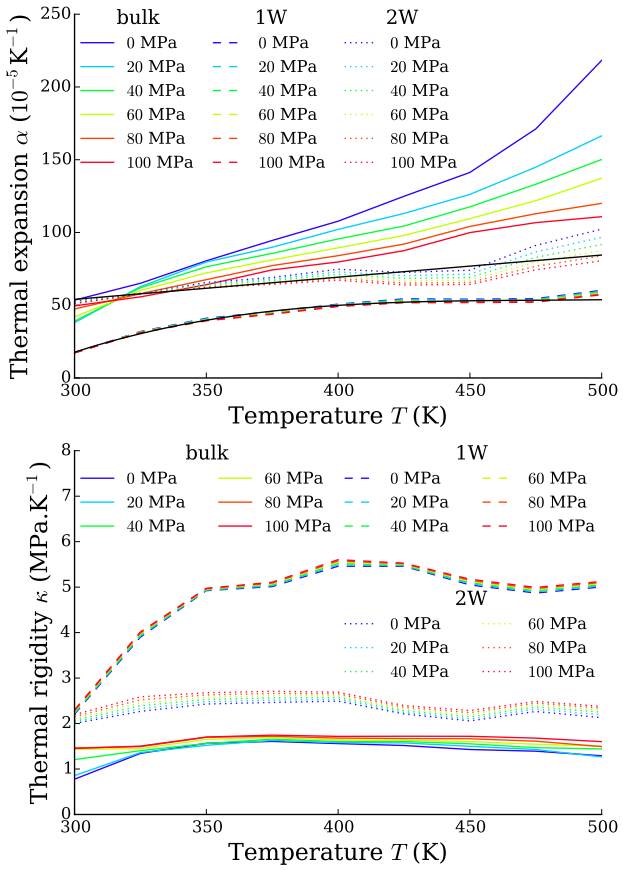

Fig. 4 Thermal expansion (top) and thermal rigidity (bottom) isobars of water SPC/E bulk and confined in Na-Montmorillonite.

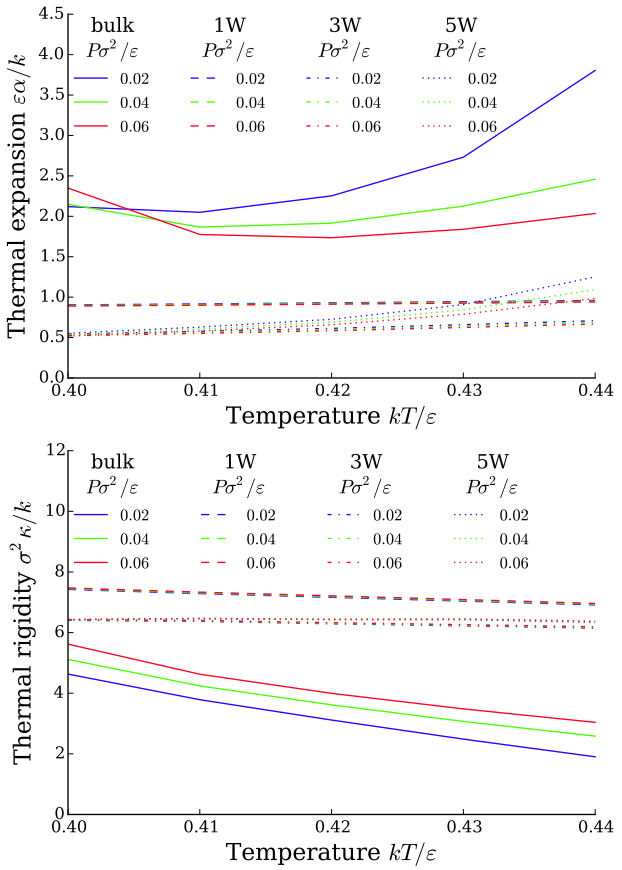

Fig. 5 Thermal expansion (top) and thermal rigidity (bottom) isobars of the LJ fluid bulk and confined in the slit pore. The results are reduced with respect to the LJ parameters σ and ε.

the domain of LJ liquid (temperatures from $0.40\varepsilon/k$ to $0.46\varepsilon/k$, and pressures up to a few times the critical pressure $P_{cr}\sigma^2/\varepsilon = 0.02$). Doing so we can confront the thermo-mechanical coupling moduli of water to that of a more 'conventional' fluid. According to these results, thermal rigidity is higher for the confined fluids than for the bulk fluids; whereas thermal expansion is smaller. It should be noted, however, that the results of water SPC/E and LJ fluids exhibit some significant differences. The confined thermal rigidity is 3 to 4 times larger than the bulk one for 1W water and 1.5 to 2 times larger for 2W water. The relative difference is less pronounced for the LJ fluid: the confined thermal rigidity is almost equal to the bulk one at low temperatures and does not exceed 2 times the bulk one at high temperatures. The confined thermal expansion is 3 to 4 times smaller than the bulk one for the LJ fluid, whereas it is almost equal or slightly smaller for water SPC/E. For both fluids, the compressibility is much smaller for the confined fluid than for the bulk fluid. Overall, the confinement increases the compressibility similarly for water SPC/E and LJ fluid, but the change in thermal properties are somehow dissimilar, in particular at low temperatures (below 400K) which are of most interest for applications. Relative to their respective bulk, thermal properties of confined water SPC/E are anomalously higher than that of the confined LJ fluid. The results of Figure 4 are consistent with the results reported by [23] for low Ca/Si C-S-H and by [28] for hydration water near model solid surfaces (see Fig. 14 for the hydrophilic cases, i.e., low values of U_0). Oleinikova and Brovchenko [28] show that confined thermal expansion correlates very well with density, which supports a purely physical origin of the properties of confined water. Overall, the confined undrained thermal expansion α_c^u exhibits some dependence on temperature, but little dependence on confined pressure. In Table 1, we adopt fits for the temperature dependence, linear for 2W water and polynomial for 1W water. The black lines in Figure 4 (top) correspond to these fits.

Let us now focus on the undrained rigidities K_c^V and K_c^N (Fig. 6). First, it is important to note that the confined water rigidities clearly differ by almost a factor

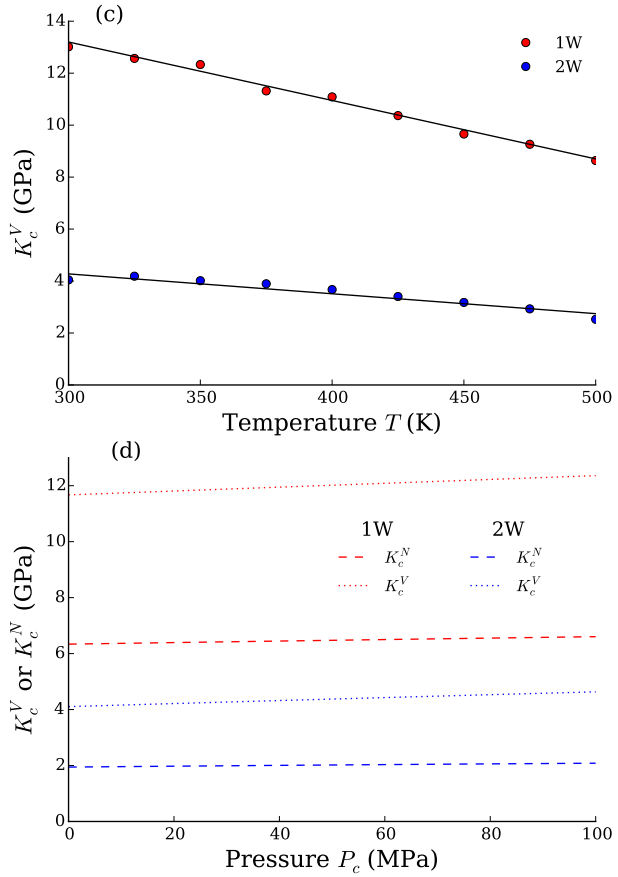

Fig. 6 Undrained rigidities of confined water in Na-Montmorillonite. (top) Evolution of K_c^V with temperature. (bottom) Evolution of K_c^V and K_c^N with confined pressure for 1W and 2W waters.

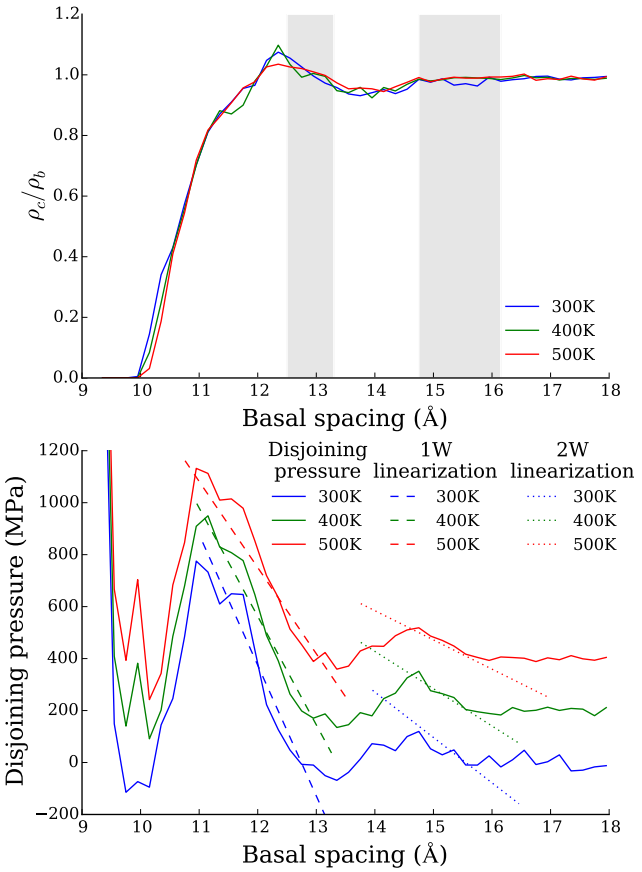

Fig. 7 Drained properties of confined water in Na-Montmorillonite. (top) Confined density relative to the bulk density as function of the basal spacing. The shaded areas correspond to the domains of 1W and 2W waters for disjoining pressures between −100 MPa and +100 MPa. (bottom) Disjoining pressure as function of the basal spacing. The linear fits of the 1W and 2W branches correspond to the values of K_c^d and α_c^d estimated. The curves at 400K and 500K are shifted up of 200MPa and 400MPa for the sake of readability.

2 which supports the analysis that Gibbs-Duhem equation does not apply to confined water (following Gibbs-Duhem equation, one would have $K_c^V = K_c^N$). Therefore, relaxing the assumption about Gibbs-Duhem equation seems necessary to rigorously capture the behavior of water confined in clays. According to Figure 6, K_c^V and K_c^N seem almost insensitive to confined pressure P_c but little sensitive to temperature T in the ranges of interest for this work (domain of liquid water). Moreover, the ratio $\delta = K_c^V/K_c^N$ appears independent of both temperature and pressure (but a little different for 1W and 2W waters). Accordingly, in Table 1, we adopt linear fits in temperature for the expression of K_c and fixed values for δ. The black lines in Figure 6 (top) correspond to the linear fit.

Finally, let us focus on the drained properties (Fig. 7). Owing to the Grand Canonical steps, the drained simulations are usually much less accurate than the undrained simulations (see Fig. 3). So, only rough estimates are achieved for the drained properties (K_c^d and α_c^d). The drained properties are roughly estimated by considering that $\gamma = \frac{K_c^V - K_c^d}{K_c^N}$ and α_c^d have fixed value, independent of temperature and pressure (but different between 1W and 2W waters). The fits obtained correspond to the dashed and dotted lines in Figure 7 (bottom), and the corresponding values are listed in Table 1. It is worth noting that the drained rigidity K_c^d and thermal expansion α_c^d exhibit non negligible values: K_c^d is of same order of magnitude as K_c^V and K_c^N, and α_c^d of same order of magnitude as α_c^u. Again, this observation confirms that Gibbs-Duhem equation is not valid for the confined water (Gibbs-Duhem equation would impose $K_c^d = 0$ and $K_c^d \alpha_c^d = 0$). Regarding the confined density ρ_c, we find it is almost equal to the bulk density ρ_b in the range of interest for the 1W and 2W domains (Fig. 7 (top)). So we adopt a value of 1 for the ratio ρ_c/ρ_b.

Property	1W water	2W water
K_c (GPa)	$7.1 - 0.012 \cdot (T - 300\text{K})$	$1.95 - 0.0035 \cdot (T - 300\text{K})$
δ	1.86	2.17
γ	1.02	0.87
α_c^u (10^{-5}K^{-1})	$6.1863 \cdot 10^{-6} \cdot T^3 - 0.0088373 \cdot T^2 + 4.2189 \cdot T - 619.60$	$0.15231 \cdot T + 8.3333$
α_c^d (10^{-5}K^{-1})	36	5
ρ_c/ρ_b	1	1

Table 1 Values and expression of the confined properties of 1W and 2W water estimated from the molecular simulation results. The temperature T is expressed in Kelvin in the expressions.

4 Application to the undrained heating experiment

Now that the confined fluid properties are known, one can apply poromechanics to the thermal pressurization experiments of Monfared et al. [26]. These experiments are performed on saturated samples of the Shaly facies of Opalinus Clay (Mont Terri laboratory) in which approximately half of the porosity is made of micropores. The mineral composition of Opalinus Clay is complex with 65% of various types of clay, out of which only smectites are swelling clays, i.e., require a poroelastic description of the adsorbed interlayer water. With no further details about the type of smectite, we use the properties of confined water obtained for Na-Montmorillonite, which is a necessary simplification with respect to the real material. The considered Na-Montmorillonite is quite typical (surface charge of -0.124 C/m^2 with substitutions randomly distributed both in the octahedral and tetrahedral layers). To the best of our knowledge the set of 6 thermo-mechanical moduli describing the drained and undrained behavior of confined water has never been estimated before. So there is no basis to confront our results, and the sensibility to the type and properties of the clay is unknown so far and is left for future works.

Hereafter, we successively consider the usual poromechanics (Eq. 3), the poromechanics extended to microporous media (Eq. 5), and the poromechanics extended to double porosity media (Eq. 8). In all cases, one has to provide the poromechanical properties of the porous solid (K, b etc...). For this purpose, Monfared et al. [26] provide the values of the drained compressibility ($\kappa_d = \frac{\partial \epsilon}{\partial \sigma}\big|_{P_{fluid},T} = 1.85 \cdot 10^{-6}$ kPa^{-1}), of the unjacketed compressibility ($\kappa_s = -\frac{\partial \epsilon}{\partial P_b}\Big|_{\sigma=-P_b,T} = 2 \cdot 10^{-8}$ kPa^{-1}), of the solid thermal expansion ($\alpha_s = 3 \cdot 10^{-5}$ K^{-1}), and of the porosity ($\phi = 0.18$) half of which are macropores and the other half micropores. Additional information is needed to fully characterize the porous solid in the double porosity case. Accordingly, we will consider two usual assumptions in soil mechanics: incompressibility of the solid $k_s \to \infty$, and iso-deformation of the micro and macro porosities (i.e., $\frac{b_b}{\phi_b} = \frac{b_c}{\phi_c}$). Apart from those two assumptions, no other assumption or fitting parameter is used in what follows. All confined water properties needed are listed in Table 1, and bulk water properties were obtained from NIST (https://webbook.nist.gov/).

Let us first apply usual poromechanics. The drained compressibility can be identified as the inverse of the bulk modulus : $K = 0.54$ GPa. For an incompressible solid, $b = 1$ and $\frac{1}{N} = 0$. The unjacketed compressibility should verify $\kappa_s = \frac{1-b}{K}$ which leads to a Biot coefficient of $b = 1 - \frac{\kappa_s}{\kappa_d} = 0.99$ very close to the assumption of incompressible solid. Note that the Biot coefficient is known to vary significantly with the confining stress [37] and is close to 1 here because the confining stress in the experiments of Monfared et al. [26] is relatively small (4.1 MPa). Integrating the thermal pressurization factor of usual poromechanics (Eq. 3), we obtain the pressurization curve displayed in Figure 8. This estimation is almost identical to that of Monfared et al. [26] (Figure 9). The usual poromechanics underestimates significantly the experimental pressurization.

Let us turn to the poromechanics extended to microporous media. The drained compressibility can be identified as the inverse of the effective bulk modulus: $K^{eff} = 0.54$ GPa, while the effective Biot coefficient is related to the unjacketed compressibility: $b^{eff} = 1 - \frac{\kappa_s}{\kappa_d} = 0.99$. Assuming incompressibility of the solid, $b = 1$ and $\frac{1}{N} = 0$ so that $b^{eff} = \gamma \frac{\rho_c}{\rho_b}$. Since $\frac{\rho_c}{\rho_b} \approx 1$ and $\gamma = 1.02$ and 0.87 for 1W water and 2W water, respectively, one gets $b^{eff} = \gamma = 1.02$ (1W) or 0.87 (2W). While the value for 1W water could be consistent with the experiment, the value for 2W water is not. This points to an inconsistency of the extended poromechanics. Any tentative parameterization of the poromechanics seems to fail. And any attempt to apply the thermal pressurization given by Equation (5) leads to results inconsistent with experiments, even worse than the estimate of usual poromechanics for the 1W water.

Let us consider finally the poromechanics extended to double porosity media. Again the drained compress-

ibility is the inverse of the effective Biot coefficient ($\tilde{K}^{eff} = 0.54$ GPa) and the effective Biot coefficient is related to the unjacketed compressibility ($b^{eff} = 1 - \frac{\kappa_s}{\kappa_d} = 0.989$). Assuming incompressibility of the solid and isodeformation of the pores, $b_b = b_c = 0.5$ and $N_{bb} = N_{cc} = -N_{bc}$. In contrast with the single porosity case, one can recover the experimental effective Biot coefficient b^{eff} from the porous solid Biot coefficient (b_b and b_c) by adjusting the value of the Biot moduli: $N_{bb} = N_{cc} = -N_{bc} = 1$ GPa. Such values of the Biot moduli are in a reasonable range. Therefore, parameterization of the extended double porosity poromechanics can be achieved consistently. Integrating the thermal pressurization coefficient of Equation (8), we obtain the thermal pressurization displayed in Figure 8 (top), where we distinguish two cases: 1W water or 2W water in the micropores. It appears that the 2W water case provides an estimate of thermal pressurization that compares well with the experiment, whereas the 1W case underestimate thermal pressurization even more than the usual poromechanics. This suggests that the micropores of the clay mostly contain 2W water, which is reasonable since 2W water is the stable confined state at the confining stress of the experiment (a few MPas), whereas 1W water is meta-stable [21]. The error bars in Figure 8 (top) quantify the uncertainty associated with the choice of micropore volume. This uncertainty is quite limited. Therefore, the use of the extended poromechanics seems to successfully capture the experimental thermal pressurization provided that the water in the micropores has properties similar to that of 2W water in Na-Montmorillonite.

A more detailed picture is given in Figure 8 (bottom), where we display the three different contributions of Equation (8) to the total pressurization coefficient. One can attribute the first contribution to the water in the macropores, and the others to the water in the micropores, but this vision is somehow biased since there are fluid transfers between the two porosity. It appears that the excess pressurization of the water in clay is mostly explained by the third contribution. This contribution is the least intuitive. It arises from the mismatch between the thermal expansion at constant bulk pressure and at constant confined pressure (see the discussion in section 2). Conversely, the second term, analogous to the pressurization of usual poromechanics but applied to the micropores, is almost negligible.

Opalinus Clay exhibits a quite strong anisotropy with a Young's modulus that can vary by a factor 3-4 depending on the loading direction [41]. Anisotropy is not accounted for in the new poromechanics presented in this paper. We discuss hereafter its importance in our analysis of undrained thermal pressurization. Adopting a tensor formulation, the poro-mechanical description of an anisotropic medium involves anisotropic elastic tensors [42, 43]. In the general case, the thermo-poro-elastic behavior is characterized by the forth order drained compliance tensor $\mathbb{C}^{-1}$ instead of the drained compressibility κ_d and shear modulus, by the second order Biot coefficient tensor $\underline{\underline{b}}$, instead of the scalar Biot coefficient, and by the second order thermal expansion tensor $\underline{\underline{\alpha}}$, instead of the scalar thermal expansion α:

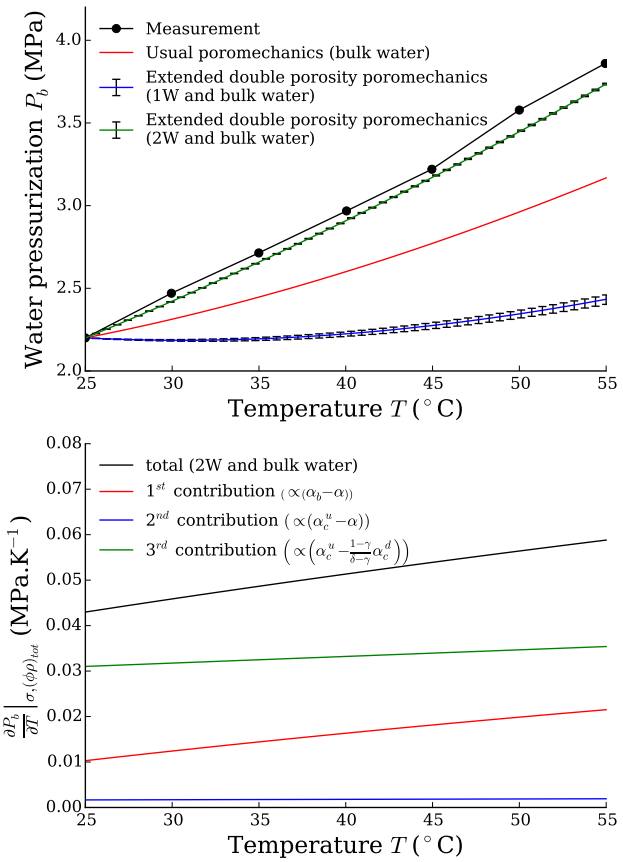

Fig. 8 (top) Application of poromechanics to the thermal pressurization experiment of [26] and comparison with the experimental results. The extended double porosity poromechanics is consistent with the experimental results considering the 2W water in the micropores. The usual poromechanics underestimates the thermal pressurization, and the extended poromechanics considering the 1W water underestimates even more. The error bars stand for the uncertainty associated with the choice of micropore volume (±0.2Å uncertainty in solid clay layer thickness). (bottom) Comparison of the three different contributions to the thermal pressurization factor (Eq. 8), in the case with 2W water in the micropores (case consistent with experiment). One can roughly view the 1^{st} contribution as that of the macropores, and the 2^{nd} and 3^{rd} as that of the micropores. The 3^{rd} contribution is the one that mostly explains the excess thermal pressurization compared to the usual poromechanics. This contribution is little intuitive, it arises from the mismatch between the thermal expansion at constant bulk pressure and at constant confined pressure.

$$\begin{cases} d\underline{\underline{\sigma}} = \mathbb{K} : d\underline{\underline{\epsilon}} - \underline{\underline{b}} dP - \mathbb{C} : \underline{\underline{\alpha}} dT \\ d\phi = \underline{\underline{b}} : d\underline{\underline{\epsilon}} + \frac{dP}{N} - \alpha_\phi dT \\ ds_s = \left(\mathbb{C} : \underline{\underline{\alpha}}\right) : d\underline{\underline{\epsilon}} - \alpha_\phi dP + \frac{c}{T} dT \end{cases} \tag{9}$$

Complete derivation of the new poromechanics in an anisotropic framework is quite tedious and is left for future work. Yet, in the particular problem of the undrained thermal pressurization experiment, the expression of pressurization with anisotropy is easily derived for the usual poromechanics and for the new poromechanics limited to single porosity media. In usual poromechanics, we have:

$$\left.\frac{\partial P_b}{\partial T}\right|_{\underline{\underline{\sigma}},\phi\rho} = \frac{\alpha_\phi + \phi\alpha_b - \underline{\underline{b}} : \underline{\underline{\alpha}}}{1/M + \underline{\underline{b}} : \mathbb{C}^{-1} : \underline{\underline{b}}} \tag{10}$$

Comparing this expression with the one for an isotropic medium (Eq. 3), one readily see that pressurization is sensitive to the most compliant direction in a strongly anisotropic medium (the term $1/M$ is one order of magnitude smaller than typical values of the weighted compressibility $\underline{\underline{b}} : \mathbb{C}^{-1} : \underline{\underline{b}}$). The drained compressibility $\kappa_d = 1/K = 1.85 \cdot 10^{-6}\text{kPa}^{-1}$ reported by Monfared et al. [26] was actually calibrated from the Skempton coefficient $B = -\left.\frac{\partial P_b}{\partial \sigma}\right|_{\phi\rho_b,T}$ measured by an undrained isotropic compression test. Monfared et al. analyzed the Skempton coefficient from the expression for an isotropic medium: $B = \frac{b/K}{1/M + b^2/K}$. But for an anisotropic medium, $B = \frac{\underline{\underline{b}} : \mathbb{C}^{-1} : \underline{\underline{1}}}{1/M + \underline{\underline{b}} : \mathbb{C}^{-1} : \underline{\underline{b}}}$. The Biot coefficient tensor is close to identity (very small unjacketed compressibility), so the drained compressibility reported by Monfared et al. actually quantifies the weighted compressibility $\underline{\underline{b}} : \mathbb{C}^{-1} : \underline{\underline{b}}$ that appears in the expression of the thermal pressurization for an anisotropic medium (Eq. 10). Accordingly, the estimation of thermal pressurization from usual poromechanics in Figure 8, remains almost the same in an anisotropic framework.

In turn, for a single porosity adsorbing medium, we have:

$$\begin{aligned} \left.\frac{\partial P_b}{\partial T}\right|_{\sigma,\phi\rho_c} =& \frac{\rho_b}{\delta\rho_c} \frac{\alpha_\phi + \phi\alpha_c^u - \underline{\underline{b}} : \underline{\underline{\alpha}}}{1/\mathcal{M}^{eff} + \underline{\underline{b}} : \mathbb{C}^{-1} : \underline{\underline{b}}} \\ &+ \frac{\rho_b}{\rho_c} \frac{\delta - \gamma}{\gamma} K_c \left(\alpha_c^u - \alpha_c^d\right) \end{aligned} \tag{11}$$

We recover, an expression similar to the isotropic case (Eq. 5), but the first term is modified to account for the anisotropy of the medium. One can note that the modification follows the same structure as in usual poromechanics (Eq. 10), and the magnitude of the first term is dominated by the most compliant direction in the weighted compressibility $\underline{\underline{b}} : \mathbb{C}^{-1} : \underline{\underline{b}}$. As before, the calibration of the effective drained compressibility, is actually based on the Skempton coefficient which takes the form $B = \frac{\rho_b}{\delta\rho_c} \frac{\underline{\underline{b}} : \mathbb{C}^{-1} : d\underline{\underline{\sigma}}}{1/\mathcal{M}^{eff} + \underline{\underline{b}} : \mathbb{C}^{-1} : \underline{\underline{b}}}$, so it captures the effect of anisotropy involved in the expression of thermal pressurization. Therefore, our estimation of the first term of thermal pressurization (Eq. 11) would remain almost the same in an anisotropic framework. Interestingly, the second term corresponding to $\left.\frac{\partial P_b}{\partial T}\right|_{P_c,\phi\rho_c}$ depends on the fluid only and is not affected by the anisotropy. As we have seen, this term is the one that mostly explains the anomalously high pressurization (Fig. 8). Although, we do not derive here the impact of anisotropy for the double porosity medium, one can anticipate similar effects, and the confrontation of Figure 8 would remain similar. In particular, the main contribution to the excessive pressurization would remain the third term of Eq. (8), i.e., the mismatch between the thermal expansions at constant P_c and at constant P_b.

5 Conclusion

Pore fluid pressurization, one of the major cause of soil instability, is anomalously high in saturated clay submitted to undrained heating. In this work, we apply a new formulation of thermo-poro-mechanics to explain this anomaly. This formulation was derived recently [5] to include the unusual effects of adsorption on confined fluids properties, and in particular the fact that Gibbs-Duhem equation is no more valid under adsorption. A major consequence is that full characterization of confined fluid thermo-mechanics requires 6 moduli instead of 3 for bulk fluids (compressibility, thermal expansion, heat capacity): one has to distinguish compressibility with respect to volume and compressibility with respect to number of molecules, and there are non negligible drained compressibility and thermal rigidity (i.e., at fixed reservoir bulk pressure, the pore pressure can still vary with the pore size and temperature). Applying this new theory requires estimating those moduli and we do so for water confined in Na-Montmorillonite by using molecular simulation. Molecular simulation estimates confirm that Gibbs-Duhem equation is not valid for water in clays, which supports the need for a poromechanics adapted to this new paradigm. Our estimates of confined water undrained thermal expansion are consistent with existing literature results for water hydration on model hydrophilic surface. Comparing the case of water to that of a model Lennard-Jones fluid in a slit pore, it appears that water exhibits a quite spe-

cific thermo-mechanical coupling at low temperatures. The undrained thermal expansion of confined water appears almost equal to that of bulk water, whereas the confined LJ fluid has a much lower thermal expansion than the bulk LJ liquid.

From the new poromechanical formulation, we derive the expression of fluid pressurization during undrained heating. The pressurization in a microporous medium involves a term analogous to that of usual poromechanics, and another term which originates from the mismatch between the thermal expansion of the fluid at constant bulk pressure and the thermal expansion at constant confined pressure. The magnitude of this second term is hard to anticipate and appears to be dominant in the case of water confined in clay. For practical application to water in clays, all the confined properties needed are listed in Table 1 (we distinguish 1W water and 2W water). Applying the new poromechanics to the pressurization experiments, we find that only the double porosity poromechanics with 2W water in the micropores provides estimates consistent with experimental results. Considering 1W water underestimates pressurization, as is the case with usual poromechanics. This result suggests that water transfers between micro- and macro-porosities are critical to explain the undrained experiment. It also suggests clay micropores contain 2W water only, which is reasonable since 2W water is the stable confined state at the conditions of the experiment. Detailed investigation shows that the main reason for the anomalous pressurization is the less intuitive contribution: the mismatch between confined thermal expansion at constant bulk pressure and at constant confined pressure.

To the best of our knowledge, this work is the first that relates quantitatively the behavior of water confined in nanometric clay layers, estimated by molecular simulation, to the macroscopic behavior of a claystone, which opens wide perspectives of applications to clay-rich materials, but also potential transposition to other adsorption-sensitive materials (cement-based materials, microporous carbons, wood, bones etc.).

Acknowledgements We gratefully acknowledge funding through the project TEAM2ClayDesicc from the French National Research Agency (Agence Nationale de la Recherche, contract ANR-14-CE05-0023-01).

Conflict of interest

The authors declare that they have no conflict of interest.

References

1. M. P. Allen and D. J. Tildesley. *Computer simulation of liquids*. Oxford University Press, 1989.
2. H J C Berendsen, J R Grigera, and T P Straatsma. The missing term in effective pair potentials. *The Journal of Physical Chemistry*, 91(24):6269–6271, nov 1987.
3. E. S. Boek, P. V. Coveney, and N. T. Skipper. Molecular Modeling of Clay Hydration: A Study of Hysteresis Loops in the Swelling Curves of Sodium Montmorillonites. *Langmuir*, 11(12):4629–4631, dec 1995.
4. Patrick A. Bonnaud, Hegoi Manzano, Ryuji Miura, Ai Suzuki, Naoto Miyamoto, Nozomu Hatakeyama, and Akira Miyamoto. Temperature Dependence of Nanoconfined Water Properties: Application to Cementitious Materials. *The Journal of Physical Chemistry C*, 120(21):11465–11480, jun 2016.
5. Laurent Brochard and Túlio Honório. Revisiting thermo-poro-mechanics under adsorption: Formulation without assuming Gibbs-Duhem equation. *International Journal of Engineering Science*, 152:103296, jul 2020.
6. Laurent Brochard, Túlio Honório, Matthieu Vandamme, Michel Bornert, and Michael Peigney. Nanoscale origin of the thermo-mechanical behavior of clays. *Acta Geotechnica*, 12(6):1261–1279, dec 2017.
7. Yuhuan Bu, Zhiyang Chang, Jiapei Du, and Dongming Liu. Experimental study on the thermal expansion property and mechanical performance of oil well cement with carbonaceous admixtures. *RSC Advances*, 7(46):29240–29254, 2017.
8. Benoit Carrier, Matthieu Vandamme, Roland J.-M. Pellenq, and Henri Van Damme. Elastic Properties of Swelling Clay Particles at Finite Temperature upon Hydration. *The Journal of Physical Chemistry C*, 118(17):8933–8943, may 2014.
9. Frederick M Chester, Christie Rowe, Kohtaro Ujiie, James Kirkpatrick, Christine Regalla, Francesca Remitti, J Casey Moore, Virginia Toy, M. Wolfson-Schwehr, S. Bose, J. Kameda, J. J. Mori, E. E. Brodsky, N. Eguchi, and S. Toczko. Structure and Composition of the Plate-Boundary Slip Zone for the 2011 Tohoku-Oki Earthquake. *Science*, 342(6163):1208–1211, dec 2013.
10. Olivier Coussy. *Mechanics and Physics of Porous Solids*. John Wiley & Sons, Ltd, Chichester, UK, jul 2010.
11. Randall T. Cygan, Jian-Jie Liang, and Andrey G. Kalinichev. Molecular Models of Hydroxide, Oxyhydroxide, and Clay Phases and the Development

of a General Force Field. *The Journal of Physical Chemistry B*, 108(4):1255–1266, jan 2004.
12. B.V Derjaguin, V.V Karasev, and E.N Khromova. Thermal expansion of water in fine pores. *Journal of Colloid and Interface Science*, 109(2):586–587, feb 1986.
13. B.V. Derjaguin, V.V. Karasev, and N.B. Ur'ev. Peculiarities of the thermal expansion of water in the pores of aerosil powder. *Progress in Surface Science*, 40(1-4):414–417, may 1992.
14. Stephen H. Garofalini, Thiruvilla S. Mahadevan, Shuangyan Xu, and George W. Scherer. Molecular Mechanisms Causing Anomalously High Thermal Expansion of Nanoconfined Water. *ChemPhysChem*, 9(14):1997–2001, oct 2008.
15. Siavash Ghabezloo. Micromechanics analysis of thermal expansion and thermal pressurization of a hardened cement paste. *Cement and Concrete Research*, 41(5):520–532, may 2011.
16. Siavash Ghabezloo, Jean Sulem, and Jérémie Saint-Marc. The effect of undrained heating on a fluid-saturated hardened cement paste. *Cement and Concrete Research*, 39(1):54–64, jan 2009.
17. Henri Gouin. Liquid nanofilms. A mechanical model for the disjoining pressure. *International Journal of Engineering Science*, 47(5-6):691–699, may 2009.
18. Emiel J M Hensen and Berend Smit. Why Clays Swell. *The Journal of Physical Chemistry B*, 106(49):12664–12667, dec 2002.
19. Loren G. Hepler. Thermal expansion and structure in water and aqueous solutions. *Canadian Journal of Chemistry*, 47(24):4613–4617, dec 1969.
20. T. Honorio, L. Brochard, and M. Vandamme. Effective stresses and estimations of the apparent Biot coefficient in stacked clay nanolayers. *Géotechnique Letters*, 8(2):1–18, mar 2018.
21. Tulio Honorio, Laurent Brochard, and Matthieu Vandamme. Hydration Phase Diagram of Clay Particles from Molecular Simulations. *Langmuir*, 33(44):12766–12776, nov 2017.
22. Jacob N. Israelachvili. Adhesion forces between surfaces in liquids and condensable vapours. *Surface Science Reports*, 14(3):109–159, feb 1992.
23. N M Anoop Krishnan, Bu Wang, Gabriel Falzone, Yann Le Pape, Narayanan Neithalath, Laurent Pilon, Mathieu Bauchy, and Gaurav Sant. Confined Water in Layered Silicates: The Origin of Anomalous Thermal Expansion Behavior in Calcium-Silicate-Hydrates. *ACS Applied Materials & Interfaces*, 8(51):35621–35627, dec 2016.
24. Yizhak Marcus. Effect of Ions on the Structure of Water: Structure Making and Breaking. *Chemical Reviews*, 109(3):1346–1370, mar 2009.
25. Laurent J. Michot, Frédéric Villiéras, Michèle François, Isabelle Bihannic, Manuel Pelletier, and Jean-Maurice Cases. Water organisation at the solidaqueous solution interface. *Comptes Rendus Geoscience*, 334(9):611–631, jan 2002.
26. M. Monfared, J. Sulem, P. Delage, and M. Mohajerani. A Laboratory Investigation on Thermal Properties of the Opalinus Claystone. *Rock Mechanics and Rock Engineering*, 44(6):735–747, nov 2011.
27. Márcio A. Murad and John H. Cushman. Thermomechanical theories for swelling porous media with microstructure. *International Journal of Engineering Science*, 38(5):517–564, mar 2000.
28. A. Oleinikova and I. Brovchenko. Thermodynamic Properties of Hydration Water around Solutes: Effect of Solute Size and WaterSolute Interaction. *The Journal of Physical Chemistry B*, 116(50):14650–14659, dec 2012.
29. Alla Oleinikova, Ivan Brovchenko, and Roland Winter. Volumetric Properties of Hydration Water. *The Journal of Physical Chemistry C*, 113(25):11110–11118, jun 2009.
30. Cedric Plassard, Eric Lesniewska, Isabelle Pochard, and André Nonat. Nanoscale Experimental Investigation of Particle Interactions at the Origin of the Cohesion of Cement. *Langmuir*, 21(16):7263–7270, 2005.
31. Klaus Schappert and Rolf Pelster. Elastic properties and freezing of argon confined in mesoporous glass. *Physical Review B*, 78(17):174108, nov 2008.
32. Klaus Schappert and Rolf Pelster. Elastic properties of liquid and solid argon in nanopores. *Journal of Physics: Condensed Matter*, 25(41):415302, oct 2013.
33. Tim J. Tambach, Peter G. Bolhuis, Emiel J M Hensen, and Berend Smit. Hysteresis in Clay Swelling Induced by Hydrogen Bonding: Accurate Prediction of Swelling States. *Langmuir*, 22(3):1223–1234, jan 2006.
34. Patricia A. Thiel and Theodore E. Madey. The interaction of water with solid surfaces: Fundamental aspects. *Surface Science Reports*, 7(6-8):211–385, oct 1987.
35. Monika Thol, Gabor Rutkai, Andreas Köster, Rolf Lustig, Roland Span, and Jadran Vrabec. Equation of State for the Lennard-Jones Fluid. *Journal of Physical and Chemical Reference Data*, 45(2):023101, jun 2016.
36. John J. Valenza and George W. Scherer. Evidence of anomalous thermal expansion of water in cement paste. *Cement and Concrete Research*, 35(1):57–66,

jan 2005.
37. O. Vincke, P. Longuemare, M. Bouteca, and J.P. Deflandre. Investigation of the Poromechanical Behavior of Shales in the Elastic Domain. In *SPE/ISRM Rock Mechanics in Petroleum Engineering*, number July. Society of Petroleum Engineers, apr 1998.
38. Hui Wang, Christian Hellmich, Yong Yuan, Herbert Mang, and Bernhard Pichler. May reversible water uptake/release by hydrates explain the thermal expansion of cement paste? Arguments from an inverse multiscale analysis. *Cement and Concrete Research*, 113(July 2017):13–26, nov 2018.
39. Shuangyan Xu, George W. Scherer, T. S. Mahadevan, and Stephen H. Garofalini. Thermal Expansion of Confined Water. *Langmuir*, 25(9):5076–5083, may 2009.
40. Shuangyan Xu, Gregory C. Simmons, and George W. Scherer. Thermal Expansion and Viscosity of Confined Liquids. *MRS Proceedings*, 790:P6.8, jan 2003.
41. Alexey Yurikov, Maxim Lebedev, Marina Pervukhina, and Boris Gurevich. Water retention effects on elastic properties of Opalinus shale. *Geophysical Prospecting*, 67(4):984–996, may 2019.
42. Yang Zhao and Ronaldo I. Borja. A continuum framework for coupled solid deformationfluid flow through anisotropic elastoplastic porous media. *Computer Methods in Applied Mechanics and Engineering*, 369:113225, sep 2020.
43. Xuejun Zhou and Ahmad Ghassemi. Biots Effective Stress Coefficient Tensor Measurements on Mancos Shale. In *53rd U.S. Rock Mechanics/Geomechanics Symposium*, pages ARMA–2019–0516. American Rock Mechanics Association, 2019.